IEICE Communications Express, Vol.13, No.4, 97–100

ComEX

LETTER

Knife-edge diffraction model for vehicle shadowing estimation in site- and scenario-specific wireless channel emulator

Siraphop Saisa-ard [1, a)], **Nopphon Keerativoranan** [1, b)], **and Jun-ichi Takada** [1, c)]

Abstract In developing a site- and scenario-specific wireless channel emulator, a computationally efficient shadowing model for vehicles is essential for dynamic emulation with constrained computational resources. In this work, a single-dominant-ray knife-edge diffraction model is proposed to approximate the overall shadowing gain from a cuboid-shaped vehicle by a single diffraction ray. The proposed model is validated with full-wave simulations at 760 MHz. The efficacy of the model is demonstrated through a comparison of the coefficient of determination with that obtained from full-wave simulations and the 3GPP rectangular screen model.

Keywords: knife-edge diffraction model, vehicular communication, vehicle shadowing, wireless channel emulator

Classification: Antennas and propagation

1. Introduction

With the advancement of 5G technology, applications that rely on high degree of connectivity, such as cyber-physical system (CPS) or vehicle-to-vehicle (V2V) communication, are expected to rapidly emerge. Therefore, a need arises for a new system verification technology that can efficiently test system performance and ensure interoperability among systems instead of traditional field testing measurement, which is time-consuming, expensive, and not reproducible. Therefore, the novel site- and scenario-specific wireless channel emulator (WCE) has gained research attention due to its application as a part of a virtual testbed for future wireless systems [1]. One of the challenges is how to handle a dynamic environment, so that the mobility of the scene, such as road traffic, is acceptably reproduced while remaining operable in real-time.

In a recent work [2], a site-specific WCE was proposed, employing the grid-based channel modeling (GBCM) technique. This technique generates and stores deterministic (e.g., ray-tracing simulation) channel parameters that reflect the characteristics of the stationary propagation environment between transmitter (Tx) and a set of reference receiver (Rx) spatially distributed in a grid structure. These parameters are interpolated to any arbitrary Rx location in the online processing to emulate the dynamic channel due to Rx mobility. However, the stored parameters do not take into account the dynamics of the environment itself, such as the motion of other systems or users. In particular, the vehicular communication channel is highly susceptible to the influence of the dynamic propagation environment in addition to site-specific statistics (e.g., path-loss exponent and delay-Doppler spread) because of low antenna height and large interacting object (i.e. blockage by vehicles that are large and metallic) [3].

To enable scenario-specific emulation, the geometry of the moving objects must be factored into the online interpolation process, without implying a large computational overhead. Although a dynamic ray-tracing simulation [4] can approximate the dynamic mechanism, it may not be feasible for WCE due to the constraints of the system and computational time. In the 3GPP standard [5], the obstructed vehicle is simplified as a floating rectangular PEC screen perpendicular to the ray. The three-ray knife-edge diffraction (3R-KED) model assumes three diffraction paths (sides and top) from the vehicle and chooses only the strongest path to calculate the shadowing gain [6]. However, determining three paths from an arbitrary set of cuboid parameters and Tx/Rx locations is not trivial because the two-dimensional projection fails in the case of oblique incidence (both elevational and azimuthal).

In this study, the single-dominant-ray knife-edge diffraction (1R-KED) model is introduced to approximate the shadowing gain from a cuboid-shaped vehicle. This model only modifies existing paths without generating additional ones and can handle the case of oblique incidence (both elevational and azimuthal), allowing compatibility with the online process in GBCM. The preliminary results were presented in [7]. To validate the proposed model, a full-wave electromagnetic simulation is conducted on the realistic vehicle shape using commercial software at 760 MHz. Furthermore, the impact of vehicle shape on shadowing characteristics is investigated by full-wave simulation of both a realistic vehicle shape and a simplified cuboid obstacle.

2. Single-dominant-ray knife-edge diffraction model

In the proposed 1R-KED model, a diffraction point (DP) is defined for each vehicle obstacle that minimizes the propagation distance without entering the cuboid surface. The concept behind this definition is to minimize the time according to Fermat's principle of least time. In the next step, the representative knife-edge is defined as a half-plane with its boundary line containing DP, orthogonal to the direct ray,

[1] School of Environment and Society, Tokyo Institute of Technology O-okayama, Meguro-ku, Tokyo 152–8550, Japan

a) siraphop-s@outlook.com

b) nopphon.keerativoranan@ap.ide.titech.ac.jp

c) takada@tse.ens.titech.ac.jp

DOI: 10.23919/comex.2023XBL0177

Received December 11, 2023

Accepted December 26, 2023

Publicized February 16, 2024

Copyedited April 1, 2024

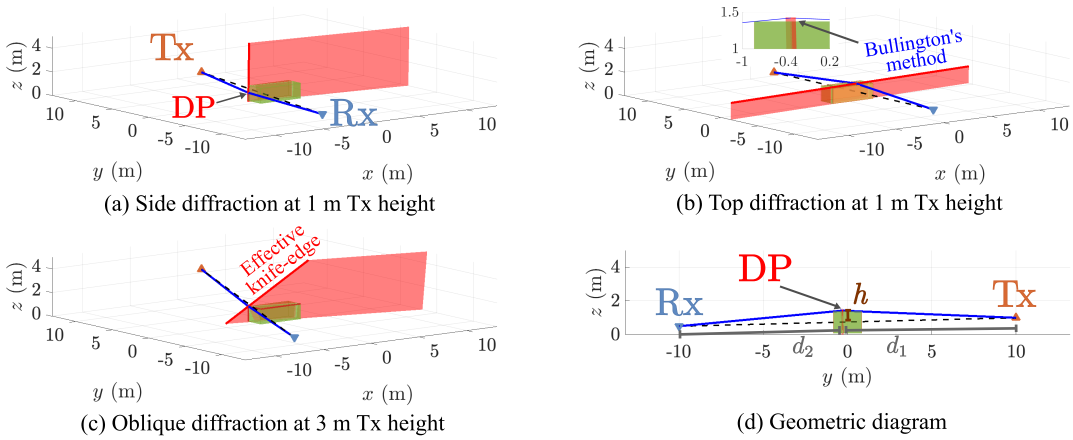

(a) Side diffraction at 1 m Tx height
(b) Top diffraction at 1 m Tx height
(c) Oblique diffraction at 3 m Tx height
(d) Geometric diagram

Fig. 1 Proposed 1R-KED model and geometric diagram

and spans toward the direct ray when the ray is blocked or away otherwise. Figure 1(a) illustrates the diffraction ray when the obstacle blocks the direct ray with DP at one of the side edges. Bullington model may be applied to address the thickness of the cuboid for the path with double diffraction. Figure 1(b) visualizes how Bullington's method is used to find a Bullington DP which is not on the cuboid surface. Figure 1(c) shows how the 1R-KED model defines the knife edge through the DP at the corner in the case of oblique incidence.

After the diffraction ray is defined, the shadowing gain is calculated in dB using the approximated knife-edge diffraction formula [8],

$$|G(\nu)|_{\text{dB}}^{\text{model}} = \begin{cases} -6.9 - 20\log(\sqrt{(\nu-0.1)^2+1}+\nu-0.1), & \text{if } \nu > -0.78 \\ 0, & \text{otherwise} \end{cases} \quad (1)$$

where $\nu = h\sqrt{2/\lambda F_e}$ is the Fresnel-Kirchhoff parameter and $F_e = (1/d_1 + 1/d_2)^{-1}$ is the equivalent focal length. h is the distance from DP to the direct ray which is positive when the direct ray is blocked. Distances from DP to Tx and Rx are indicated as d_1 and d_2, respectively, as depicted in Fig. 1(d).

3. Validation by full-wave electromagnetic simulation

The proposed 1R-KED model was validated in 7 scenarios with the shadowing gain derived from the simulation in commercial software Ansys HFSS of vehicle obstacle using the integral equation solver. In scenario 1 which is the benchmark, the vehicle is positioned at the origin facing toward $+x$ direction, and Tx is positioned 10 m away in $+y$ at 1 m height. The electric field is observed along the Rx trajectory at 0.5 m height as depicted in Fig. 2(a) to simulate the vehicle shadowing event when Tx and Rx are stationary and the vehicle moves in between. The ground is modeled as an infinite PEC plane at $z = 0$ in Figs. 2(b) - 2(c) (brown). Toyota Prius model shown in Fig. 2(b) was used in the simulation as the ground truth. The cuboid obstacle (bounding cuboid of vehicle) used in the simulation to measure the model efficacy and the effect of vehicle shape is shown in Fig. 2(c). The detailed simulation parameters are presented in Table I. In scenarios 2 - 7, the Tx-Rx distance (ρ_1), Tx-vehicle distance

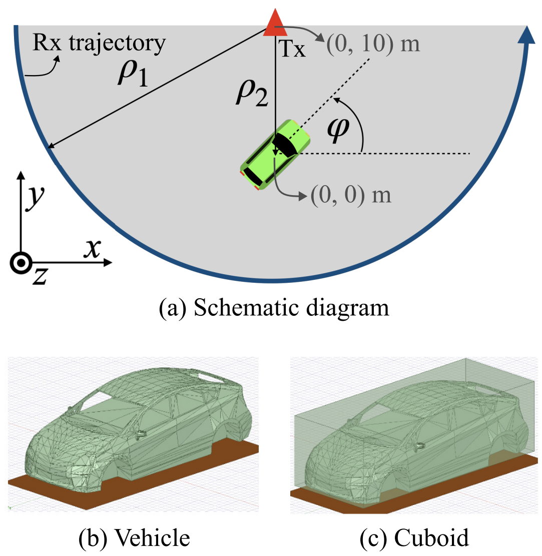

(a) Schematic diagram
(b) Vehicle
(c) Cuboid

Fig. 2 Simulation scenario

Table I Simulation parameters

Parameters	Values
Radio system	
Frequency	760 MHz
Antenna	Vertical electric Hertzian dipole
Rx height	0.5 m
Vehicle geometry	
Model	Toyota Prius
Size	$4.181 \times 1.678 \times 1.275$ m^3
Hover height	0.1 m

Table II Parameters setting at each scenario

No.	Tx height (m)	ρ_1 (m)	ρ_1 (m)	φ (deg)
1	1	20	10	0
2	**2**	20	10	0
3	**3**	20	10	0
4	1	**40**	**20**	0
5	1	**30**	**20**	0
6	1	20	10	**45**
7	1	20	10	**90**

*varied parameter is indicated in **bold**

(ρ_2), and vehicle yaw angle (φ) are varied from scenario 1 as listed in Table II.

The shadowing gain in dB is calculated from the simulated

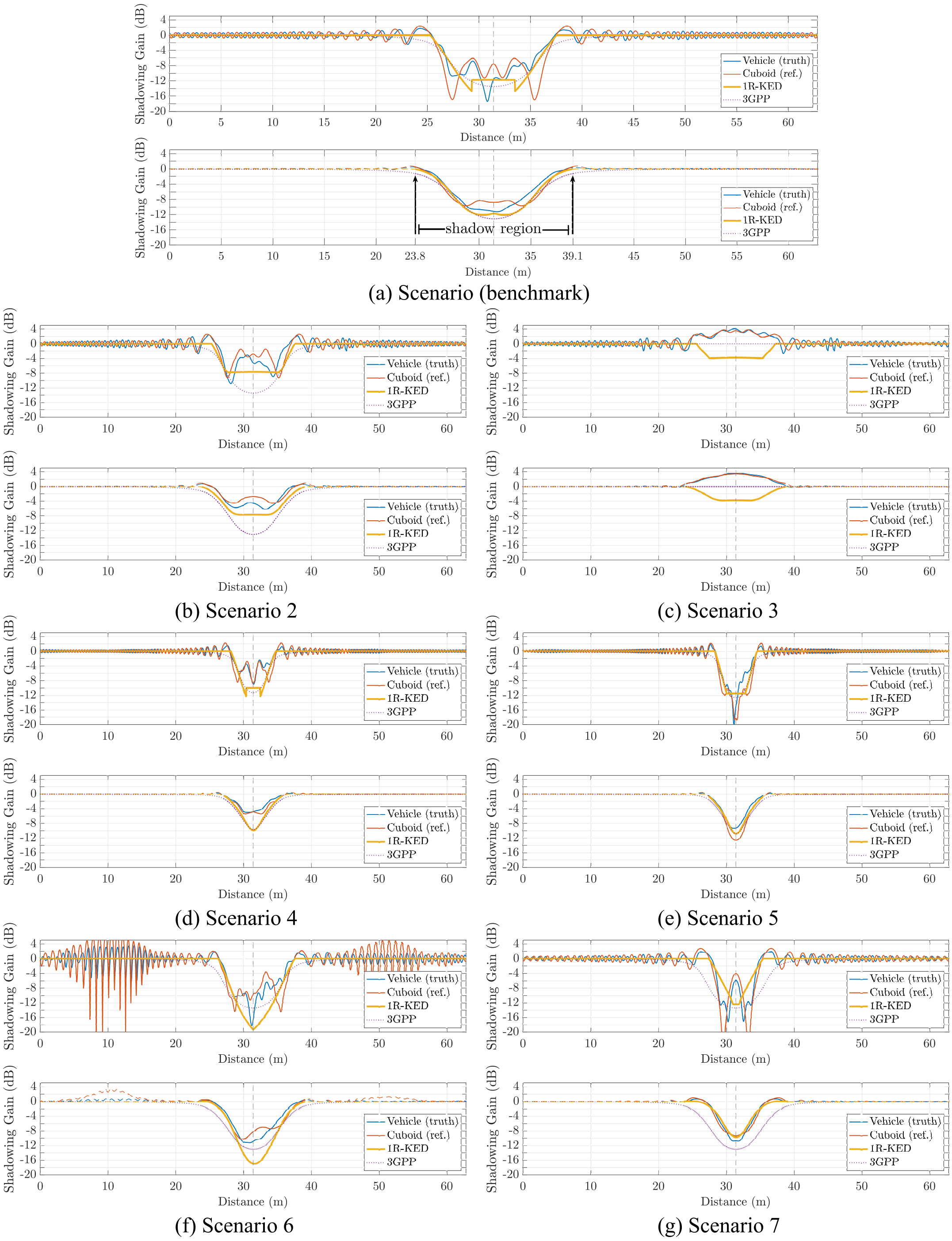

Fig. 3 Shadowing gain (without and with MA) of 1R-KED and 3GPP model in each scenario

complex electric field in Ansys HFSS as a comparison with the field without an obstacle,

$$|G(\nu)|_{\mathrm{dB}}^{\mathrm{truth}} = 20\log_{10}\left|\frac{E_{\mathrm{s}}^{z} + E_{\mathrm{i}}^{z}}{E_{\mathrm{i}}^{z}}\right|, \tag{2}$$

where E_{s}^{z} is the vertically polarized scattered field simulated by HFSS, and E_{i}^{z} is the vertically polarized incident field in free-space. Since the observation trajectory is a semi-circle around Tx with constant elevation angle, E_{i}^{z} is constant, the effect of the antenna pattern is not included.

4. Results and discussion

The shadowing gain estimated by the 1R-KED model is plotted along the Rx trajectory in Fig. 3 with the gain derived from the simulations in HFSS for vehicle and cuboid obstacle. As depicted in the upper sub-figures, the results produced from the full-wave simulation include both shadowing and fast-fading components in the gain profile. Therefore, 10λ moving average (MA) is applied to produce only the shadowing component profile and is presented in the lower sub-figures. The shadow region along the trajectory is defined as where any part of the cuboid is within 60% of the first Fresnel zone (a solid line in the lower sub-figures), whereas non-shadow region is depicted by a dashed line. The 3GPP Blockage B model [5] is presented for comparison by simplifying the vehicle into the rectangular obstacle with the size of $4.2 \times 1.3\ \mathrm{m}^2$ perpendicular to the direct ray.

The coefficient of determination (R^2) is used as the metric to evaluate each model with the ground truth calculated by:

$$R^2 = 1 - \frac{\sum_{\text{shadow}}(|G|^{\text{model}} - |G|^{\text{truth}})^2}{\sum_{\text{shadow}}(|G|^{\text{truth}} - \overline{|G|^{\text{truth}}})^2}, \quad (3)$$

where $|G| = 10^{|G|_{\text{dB}}/10}$ is the shadowing gain in linear scale with $\overline{|G|}$ being its average. This R^2 in linear scale presented in Table III emphasizes the error in shallow shadow which is more meaningful than the error in deep shadow, and is summed over the shadow region only. R^2 of cuboid simulation is calculated to examine the impact of vehicle shape in which large R^2 denotes less significance.

The scenario 1 in Fig. 3(a) depicts the benchmark result for the investigation of the effect of angle of elevation, propagation distance, and vehicle orientation. The discrepancy between the cuboid-shaped and the reference vehicles indicates the effect of shape simplification, especially during transition regions approximately at 25 - 28 m and 35 - 38 m distance. The piecewise transition in 1R-KED at distances of 29 and 33 m is due to the transition of the dominant ray path. The 1R-KED cannot reproduce the fading ripple as it is omitted by approximate KED model. After removing the fast fading as in the lower sub-figures, the shadowing profile of the proposed 1R-KED becomes more similar to that of the reference. Higher R^2 of 0.95 and 0.88 in cases with and without MA, respectively, has validated the performance of the 1R-KED, which also has a level of R^2 similar to that of the cuboid-shaped vehicle. Although the 3GPP blockage B model shows good resemblance, it has the lowest R^2 due to a 2-dB gap during the shadow region transition at 23 - 26 m and 36 - 39 m.

By increasing the height of the Tx to 2 m, 1R-KED fits well with both the reference vehicle and the cuboid vehicle in the shallow shadow region, while 3GPP shows a larger gain discrepancy, as shown in Fig. 3(b). However, with a Tx height of 3 m, the 1R-KED incorrectly produces a negative path gain as opposed to a positive gain in both reference and cuboid-shaped vehicles, as depicted in Fig. 3(c). This is possibly due to constructive interference from multiple diffraction paths that could not be produced by 1R-KED. By increasing the distances twice ρ_1 and ρ_2, the constructive gain near the shadowing center is also observed for both the reference and the cuboid-shaped vehicles, as shown in Fig. 3(d), resulting in a lower R^2 in the 1R-KED. However, with different combinations of ρ_1 and ρ_2, such constructive interference may disappear, as in Fig. 3(e) and R^2 of the proposed 1R-KED greatly improves to a level similar to that of the benchmark scenario 1. Finally, 1R-KED shows a good result with vehicle orientation variation in Figs. 3(f) - 3(g) in contrast to 3GPP which assumes a fixed-size screen obstacle. These results have validated the applicability of the proposed 1R-KED to reproduce the shadowing gain for WCE and its limitations for handling constructive interference. Note that the proposed method may be applicable with other obstacle shapes, yet requires further validation.

Table III Coefficient of determination (R^2) in each scenario

No.	Raw			Moving average		
	Cub.	3GPP	1R-KED	Cub.	3GPP	1R-KED
1	0.9	0.61	**0.88**	0.93	0.73	**0.95**
2	0.75	0.1	**0.58**	0.88	-0.02	**0.61**
3	0.77	**-2.57**	-6.88	0.95	**-4.05**	-10.8
4	0.73	0.33	**0.64**	0.85	-0.2	**0.3**
5	0.87	0.62	**0.88**	0.87	0.68	**0.92**
6	0.87	0.44	**0.86**	0.94	0.53	**0.92**
7	0.8	-0.33	**0.76**	0.97	-0.25	**0.95**

*higher R^2 between 3GPP and 1R-KED is indicated in **bold**
*Cub. : full-wave simulation of the cuboid-shaped vehicle

5. Conclusion

This paper proposes the 1R-KED model, which uses KED theory to estimate the shadowing gain of the vehicle for the site- and scenario-specific WCE. The model is evaluated at 760 MHz by comparing with the full-wave simulations of cuboid and vehicle obstacle showing satisfactory agreement in most cases. The impact of the cuboid representation on the shadowing component is shown to be minor at shallow shadow. It performs well with electrically large obstacles and is robust to vehicle rotation. However, performance significantly degrades when constructive interference occurs during the shadowing event due to multiple diffraction paths.

Acknowledgments

This research is supported by the Ministry of Internal Affairs and Communications of Japan under the contract “R&D for the realization of high-precision radio wave emulator in cyberspace” (JPJ000254).

References

[1] F. Kojima, T. Miyachi, T. Matsumura, H. Sawada, H. Harai, and H. Harada, “A large-scale wireless emulation environment with interaction between physical and virtual radio nodes for beyond 5G systems,” 2022 IEEE 33rd PIMRC, pp. 1–6, 2022. DOI: 10.1109/PIMRC54779.2022.9977562

[2] N. Keerativoranan and J. Takada, “Site-level deterministic channel emulator: Grid-based architecture and continuous channel emulation technique,” 2022 16th EuCAP, pp. 1–5, 2022. DOI: 10.23919/EuCAP53622.2022.9769688

[3] W. Viriyasitavat, M. Boban, H.-M. Tsai, and A. Vasilakos, “Vehicular communications: Survey and challenges of channel and propagation models,” *IEEE Veh. Technol. Mag*., vol. 10, no. 2, pp. 55–66, 2015. DOI: 10.1109/MVT.2015.2410341

[4] D. He, B. Ai, K. Guan, L. Wang, Z. Zhong, and T. Kürner, “The design and applications of high-performance ray-tracing simulation platform for 5G and beyond wireless communications: A tutorial,” *IEEE Commun. Surveys Tuts*., vol. 21, no. 1, pp. 10–27, 2019. DOI: 10.1109/COMST.2018.2865724

[5] 3GPP, “Study on channel model for frequencies from 0.5 to 100 GHz,” Tech. Rep., TR 38.901, ver. 16.1.0, 2019.

[6] M. Boban, J. Barros, and O.K. Tonguz, “Geometry-based vehicle-to-vehicle channel modeling for large-scale simulation,” *IEEE Trans. Veh. Technol*., vol. 63, no. 9, pp. 4146–4164, 2014. DOI: 10.1109/TVT.2014.2317803

[7] S. Saisa-ard, N. Keerativoranan, and J. Takada, “Vehicle shadowing modeling for deterministic channel emulator and electromagnetic simulation-based validation,” URSI GASS 2023, pp. 1–4, 2023. DOI: 10.46620/URSIGASS.2023.3581.ERKK6299

[8] “Propagation by diffraction,” Recommendation ITU-R P.526-15, 2019.